International Conference on Space Optics—ICSO 2008

Toulouse, France

14–17 October 2008

Edited by Josiane Costeraste, Errico Armandillo, and Nikos Karafolas

Temporal hypertelescope

F. Reynaud

L. Delage

S. Olivier

International Conference on Space Optics — ICSO 2008, edited by Josiane Costeraste, Errico Armandillo, Nikos Karafolas, Proc. of SPIE Vol. 10566, 1056601 · © 2008 ESA and CNES
CCC code: 0277-786X/17/$18 · doi: 10.1117/12.2308213

TEMPORAL HYPERTELESCOPE

F. Reynaud, L. Delage and S. Olivier

XLIM Département Photonique, UMR CNRS 6172, 123 Av. A. Thomas, 87060 LIMOGES (France),
E-mail:francois.reynaud@xlim.fr

ABSTRACT

The possibility of direct imaging is a very attractive alternative if compared to the conventional coherence analysis achieved in telescope arrays like VLTI.
A. Labeyrie has proposed the concept of hypertelescope with the key step of pupil densification. This proposal faces the difficulty to implement homothetic pupils and requires a complex architecture with sub micrometric accuracy to make the pupil reconfigurable. In this talk we propose a new version of hypertelescope devoted to high-resolution direct imaging. By using a temporal versus spatial optical-path modulation in a multi-aperture interferometer, we show that the beam densification process can be similarly achieved in the time domain giving rise to a very good reconfiguration versatility. Reducing the span of optical modulations allows us to convert this instrument into a nulling interferometer. Our new experimental configuration allows an easy and versatile recombination reconfiguration for a ground or space instrument and answers the problem of the variable spatial Fourier spectrum sampling either with a ground-based observation or with a pupil reconfiguration for a space mission. First results on a demonstration breadboard are proposed and future developments are discussed.

1. INTRODUCTION

The hypertelescope proposals [1;2] use simultaneously a homothetic reconfiguration according to the "golden rule of imaging interferometers" [3] and a pupil densification. This last step can be achieved either in the pupil or in the image plane. By this way, an angular magnification and a concentration of the energy around the zero order of the interfering beams allow to optimize the detection properties in a field of view where, for instance, an exoplanet is expected. Conclusively the performances of a temporal versus spatial telescope have to be compared in term of homothetic reconfiguration and beam densification. The versatility
of the time domain solution is discussed in order to propose an attractive evolution of the classical hyper telescope. In the first part, thanks to the spatial approach, experimentally demonstrated by [4;5], we propose the temporal version of such an instrument. In the second part we focus our talk on the advantages of a time modulated version of this imaging instrument. A versatile reconfiguration and a very high densification are the two main improvement features. At last, we show how to convert the imaging instrument into a nulling interferometer thanks to a higher densification potential in the time domain.
We conclude by an experiment providing the first demonstration of this concept with a 8 telescope aperture in a fibre linked version.

2. THEORETICAL RECALLS ON SPATIAL HYPERTELESCOPE

This paragraph is based on the proposal of A. Labeyrie or its pupil plane version so called IRAN [2;6]. The analytical description is quite different but the global results and properties could be derived similarly. Figure 1 recalls the global structure of a hypertelescope as proposed by A. Labeyrie.

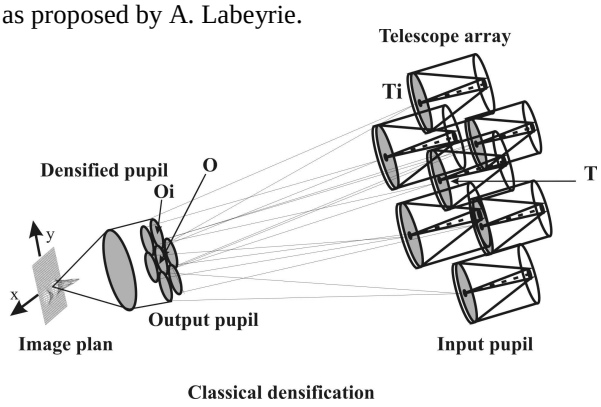

Figure 1 Classical scheme of a spatial hypertelescope.

This simplified drawing does not detail the reconfiguration and densification process but shows the main idea. This technique requires to remap the input pupil taking care to achieve this geometrical contraction using a homothetic process for the location of beams centres in the output pupil according to the "golden rule of imaging interferometry". Denoting γ the reconfiguration ratio, the distance between telescope $\mathbf{T_i}$ and the centre of the input pupil $\mathbf{T}$ is related to the position vector $\mathbf{OO_i}$ of the sub pupil $\mathbf{i}$ in the output pupil by: $\mathbf{TT_i} = \gamma \mathbf{OO_i}$ where $\mathbf{O}$ is the

output pupil origin. The γ factor gives the angular magnification of the instrument.
In order to concentrate the energy around the focal point of the image plan, each beam diameter is expanded up to the limit of an overlapping between the different sub pupils in the output pupil plan. Figure 2 illustrates this configuration.

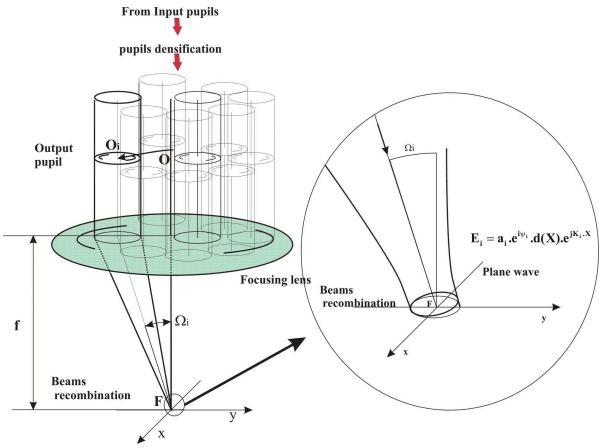

Figure 2: Beam i contribution in the image plane. The optical field has a limited plane wave structure with a diffraction envelope d(X).

Observing beam **i**, the vector $\mathbf{TT_i}$ describes the telescope position in the input pupil plane gives rise to the obliquity of the limited plane wave illuminating the image plane. Assuming the paraxial conditions to be applied, the corresponding two dimensional angle Ω_i is equal to:

$$\Omega_i = \frac{\mathbf{OO_i}}{\mathbf{f}}$$

where **f** is the focal length of the focusing lens. In the image plane, the related limited plane wave can be expressed as:

$$\mathbf{E_i} = \mathbf{a_i} e^{j\psi_i} \mathbf{d(X)} e^{j(\mathbf{K_i}.\mathbf{X})} \quad \text{(eq 1)}$$

With $$\mathbf{K_i} = \frac{2\pi}{\lambda}.\frac{\mathbf{TT_i}}{\gamma.\mathbf{f}}$$

where $\mathbf{a_i}$ and ψ_i are the modulus and input phase of beam **i**. **X** is the position vector in the image plane with two coordinates **x** and **y** (**X=(x;y)**). In the Labeyrie's configuration $\mathbf{d(X)}$ denotes the spot field envelop resulting from the diffraction of one sub pupil (see figure 2) and is supposed to be identical for all beams. The last term $e^{j(\mathbf{K_i}.\mathbf{X})}$ is related to the linear variation of the phase in the image plan according to α_i and β_i slope coefficients.

$\mathbf{K_i} = 2\pi(\alpha_i;\beta_i)$ with $\alpha_i = \frac{(\mathbf{OO_i})_x}{\lambda \mathbf{f}}$ and $\beta_i = \frac{(\mathbf{OO_i})_y}{\lambda \mathbf{f}}$

Where $(\mathbf{OO_i})_x$ denotes the projection of vector along x axis. By this way, each position $\mathbf{TT_i}$ of telescope drives the slope $(\alpha_i;\beta_i)$ of the wave front reaching the image plane. The phase variation $\varphi_i(\mathbf{x};\mathbf{y})$ is linear with an offset depending on the **y** coordinate and can be analysed along different axes parallel to the **x** axis:

$$\varphi_i(\mathbf{x}) = 2\pi(\alpha_i.\mathbf{x} + \beta_i.\mathbf{y}) = 2\pi\alpha_i.\mathbf{x} + \varphi_{i0}(\mathbf{y})$$

As demonstrated by A. Labeyrie, the possibility to retrieve the image results from the coherent superposition of these different limited plane waves and the convolution of the resulting Point Spread Function (PSF) with the object intensity distribution. The PSF is the overall intensity of the coherent superposition of fields $\mathbf{E_i}$ in the image plane. At the beginning, we will consider the $\mathbf{a_i}$ coefficients to be identical (set to one for example) and the ψ_i phase terms in the equation (eq 1) equal to 0.

$$\mathbf{PSF(X)} = \left|\sum_i \mathbf{E_i}\right|^2 = \left|\sum_i \mathbf{d(X)}.e^{j\mathbf{K_i};\mathbf{x}}\right|^2$$

$$= |\mathbf{d(X)}|^2.\left|\sum_i e^{j\mathbf{K_i};\mathbf{x}}\right|^2$$

If in the Labeyrie's configuration, $\mathbf{d(X)}$ corresponds to the sub pupil far field, in the IRAN proposal this term would be replaced by the sub-pupil function itself. In the both cases this envelope term is responsible of the phase modulation range in the recombining plane. This is directly related to the optics dimension and will not be easy to adjust in a real experiment.
For a tilted point like source illuminating the telescope array with a $\boldsymbol{\theta} = (\theta_x;\theta_y)$ obliquity, the amplitudes $\mathbf{a_i}$ remain constant but the phase ψ_i becomes:

$$\psi_i = \frac{2\pi}{\lambda}(\mathbf{TT_i}.\boldsymbol{\theta})$$

The total phase carried by the $\mathbf{E_i}$ field can be written in the image plane as:

$$\psi_i + \varphi_i = \frac{2\pi}{\lambda}(\mathbf{TT_i}.\boldsymbol{\theta}) + \frac{2\pi}{\lambda}\left(\frac{\mathbf{TT_i}}{\lambda \mathbf{f}}.\mathbf{X}\right)$$

This additional ψ_i term induces a shift of the corresponding intensity distribution:

$$\mathbf{I_\theta(X)} \approx \mathbf{PSF}(\mathbf{X} + \gamma \mathbf{f} \boldsymbol{\theta})$$

For an extended object, the incoherent superposition of the different contribution of the object $\mathbf{O}(\boldsymbol{\theta})$ leads to the image:

$$\mathbf{I(X)} = \int_{\text{object}} \mathbf{O(\theta).PSF(X + \gamma.f.\theta)d\theta}$$

Denoting $\mathbf{X_0 = f\theta}$, the image appears as a pseudoconvolution of the object intensity distribution with the point spread function:

$$\mathbf{I(X)} = \int_{\text{object}} \mathbf{O}\left(\frac{\mathbf{X_0}}{\mathbf{f}}\right)\mathbf{.PSF(X + \gamma.X_0)d\theta} \quad (2)$$

Any process able to achieve such recombination will provide an image with the same basic properties. The next paragraph demonstrates the possibility to obtain such result in the time domain. Note that the transposition in the time domain of the IRAN proposal could be achieved as well as in the Labeyrie's configuration with minor differences.

2. FROM A SPATIAL TO A TEMPORAL INSTRUMENT

The aim of this paragraph is to demonstrate the equivalence between the temporal and spatial approaches. According to the design of the experimental set up, an interferometric signal can be displayed as a function of time or space depending on whether the interferometric mixing has been achieved in a multiaxial or coaxial configuration. This point is illustrated in figure 3 for a two dimensional representation. The two techniques are fully equivalent as long as the numbers of spatial or temporal samples are identical and if the full integration times are the same for the two experimental configurations.

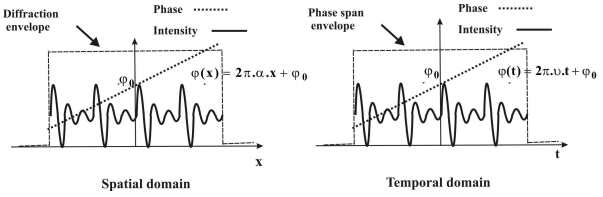

Fig 3: Analogy between spatial and temporal interferences. In the first case (left) the fringes are displayed as a function of a position x and the interferometer induces a spatial phase variation.
In the second case (right) a temporal optical path modulation allows an observation as a function of time t. The frame in which fringes are observed results respectively from a diffraction spot dimension (left) and a limited optical path stroke (right).

For classical spatial hypertelescopes, the linear phase modulations $\boldsymbol{\varphi_i(x) = 2\pi\alpha_i.x + \varphi_{i0}(y)}$ result from a variable optical path different related to the $\boldsymbol{\Omega_i}$ tilts of the optical fields $\mathbf{E_i}$ reaching the observation plane and coming from beam **i**. In the temporal case, the phase modulation $\boldsymbol{\varphi_i(t)}$ can be generated thanks to an optical path variation induced by optical path modulators. They have to be linearly actuated as a function of time as shown in figure 4.

$$\boldsymbol{\varphi_i(t) = 2\pi.\upsilon.t + \varphi_{i0}(y)} \quad (3)$$

The use of temporal frequencies $\boldsymbol{\upsilon_i}$ proportional to the slopes $\boldsymbol{\alpha_i}$ allows a complete equivalence between spatial and time domain schemes. For this purpose, the frequency $\boldsymbol{\upsilon_i}$ of the phase modulation has to be selected as proportional to the $\boldsymbol{\alpha_i}$ coefficient with an $\mathbf{A} = \frac{\boldsymbol{\upsilon_i}}{\boldsymbol{\alpha_i}}$ proportional factor.

$$\boldsymbol{\nu_i} = \mathbf{A}\frac{\mathbf{(OO_i)_x}}{\boldsymbol{\lambda}.\mathbf{f}} = \mathbf{A}\frac{\mathbf{(TT_i)_x}}{\mathbf{f}.\boldsymbol{\lambda}.\boldsymbol{\gamma}}$$

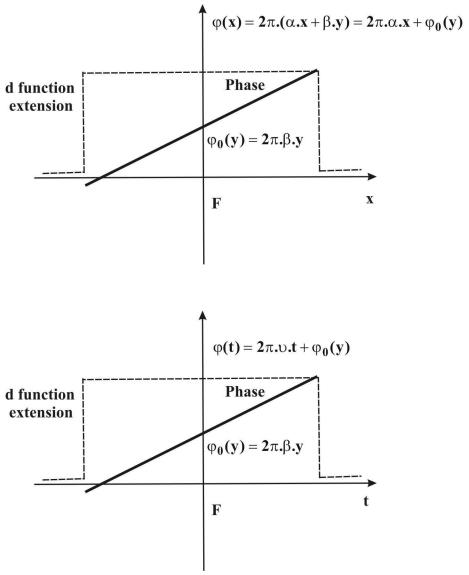

Fig 4: Phase variation of one beam for spatial and temporal modulations. Using proportional slopes between the two configurations allows to display similar interferences patterns with only a scale ratio between the two horizontal axes. The phase span is respectively driven by the diffraction effect and the optical path stroke.
Following this spatial to temporal transposition the optical field

$$\mathbf{E_i(x) = a_i e^{j\psi_i} d(X) e^{j(2\pi\alpha_i.x+\varphi_{i0}(y))}}$$

can be replaced by :

$$\mathbf{E_i(t) = a_i e^{j\psi_i} d(t) e^{j(2\pi\nu_i.t+\varphi_{i0}(y))}}$$

$\mathbf{d(t)}$ function allows to limit the phase variation as necessary. The coherent superposition of all the beams can be analyzed along **x** axis. The **A** factor gives the relationship between the spatial parameter **x** and time **t.**

$$\mathbf{x = A.t}$$

As in the spatial domain, the image is obtained by using the temporal PSF given by:

$$\mathbf{PSF(t;y) = \left|\sum_i E_i\right|^2 = \left|\sum_i d(t).e^{j(2\pi\nu_i t+}\right|^2 = |d(X)|^2.\left|\sum_i e^{jK_i;x}\right|^2}$$

For a tilted point like source with a $\boldsymbol{\theta = (\theta_x;\theta_y)}$ obliquity, the total phase of the $\mathbf{E_i}$ field becomes:

$$\boldsymbol{\psi_i + \varphi_i = \frac{2\pi}{\lambda} TT_i.\theta + \frac{2\pi}{\lambda} TT_i.(A.t;y)}$$

As Like previously, the corresponding intensity distribution is a shifted PSF:

$$\mathbf{I_\theta(At;y) = PSF[(A.t;y) + \gamma.f.\theta]}$$

The incoherent superposition of the different contribution of the object **O** leads to the full image:

$$\mathbf{I(At;y) = \int O(\theta).PSF([(A.t;y) + \gamma.f.\theta)d\theta}$$

As previously mentioned, the image appears as a pseudoconvolution of the object intensity distribution with the point spread function but now this one is displayed as a function of time. This result, which demonstrate the full equivalence between spatial and temporal display, is illustrated in figure 5

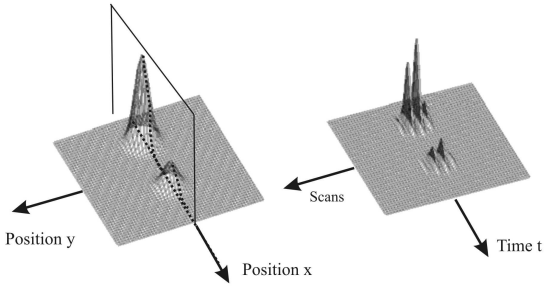

Fig 5: Temporal display versus spatial display. The two-dimensional spatial display can be replaced by a temporal one. As long as time is a one dimensional parameter, a raster scan is necessary to retrieve a time multiplexed image like on a video monitor.

In order to show a two dimensional image, the $\boldsymbol{\varphi_{i0}(y)}$ phase is modified step by step so as to display successively the different section of the image using a set of scans. The information provided along the **x** axis at a given position **y** is fully equivalent to the one observed as a function of time **t** for the scan related to the same $\boldsymbol{\varphi_{i0}(y)}$ value. The image is temporally multiplexed using a raster scan. It can be notice that in the spatial domain, the **x** span is determined by the diffraction field distribution related to the sub pupil geometry. In the temporal domain, the field of investigation is determined by the phase modulation extension directly driven by the span of the optical path modulator. It can be adjusted very easily and reduced up to zero contrary to the spatial configuration where the limitation results from the beam dimensions.

3 VERSATILITY OF THE TEMPORAL VERSION OF HYPERTELESCOPES

For a ground mission the classical hypertelescope technique faces the necessity to continuously reconfigure the densified apertures due to the earth rotation. The telescope spatial distribution, as seen from the scientific target, is continuously modified making the output pupil reconfiguration necessary as long as hypertelescopes use a homothetic reconfiguration of the sub-pupil centres. For a space mission, the reconfiguration of the input pupils map is of high interest. That makes necessary a continuous output pupil reconfiguration. This hardware operation is quite complex and spends a lot of time in a classical configuration. Conversely, in the time domain, the change of the input pupil configuration can be easily obtained by is followed by a simple change of optical path modulation slopes and offsets according to the equation (3). This operation can be achieved using the software monitoring of the optical path servo control systems. For a space mission the opportunity to change the input pupil configuration can be easily investigated thanks to this experimental functionality. By this way it is possible to take advantage of this versatility to use the redundant or non redundant configurations according to the (faint; extended) or (bright; sharp) science targets [7]. The second advantage deals with the easy control of the optical path span related to a high densification potential. In the spatial domain, the phase span is determined by the slope of the wave front and diffraction spot diameter over which the beam is spread. The spatial densification process being limited by the overlapping of sub-apertures in the output plan,

the span limit results from the diffraction pattern of each sub pupil. Conversely, in the time domain, the full variation of the phase can be reduced as much as necessary by reducing the span of the optical path modulation. By this way, it is possible to focus the investigation on a limited part of the field. This point is illustrated in figure 6. The servo control system is adjusted in order to limit the scan, this operation being achieved by software. This functionality can be investigated up to a zero optical path modulation. In a such configuration, the instrument is pointing only one point of the image (see right part of figure 6)

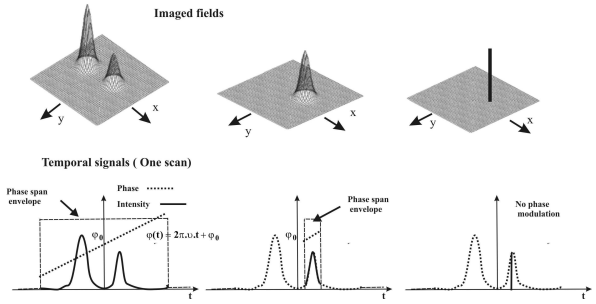

Fig 6: The optical path stroke on each modulator can be adjusted in order to modify the field over which the image is displayed (from left to right). Reducing these modulations allows concentrating this imaging process on a limited area. Setting the different phases to the proper values enables to operate in a nulling configuration (right) analyzing only one point of the scene to be observed. In this case, the instrument is operating as a nulling interferometer [8]. The light coming from a planet can be selected in the point of the field, while the light of its parent star is nullified.

4 IMPLEMENTATION OF A TEMPORAL HYPERTELESCOPE; PRELIMINARY RESULTS

A time modulated version of a hypertelescope can be drawn as proposed in figure 7.

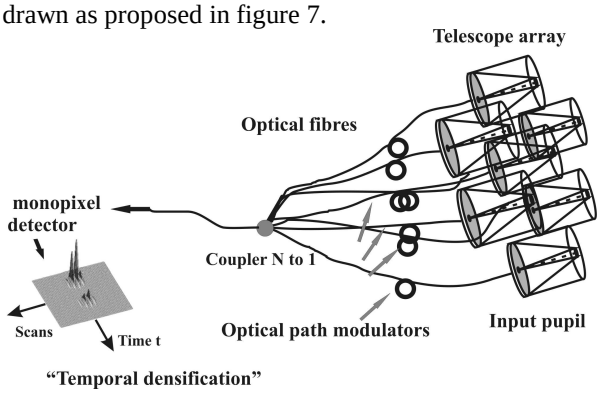

Fig 7: Proposal for a temporal hypertelescope using optical fibres and a guided coupler acting as a combiner. The optical path modulators induce the phase variations necessary to form an image. The image is temporally multiplexed. This sketch uses optical fibres to propagate the light all over the interferometric arms but classical processes using mirror trains, air delay lines and classical beam splitters can be equivalently used. The light is picked at the N telescope foci and passes through optical path modulators before being recombined using a N to one beam combining coupler in a coaxial configuration. The convenient phase modulations are obtained by using optical fibre stretchers inducing an optical path variation. Servo control systems have been developed for such kind of applications [9;10] and can monitor, with a nanometric accuracy, the linearity of the optical path variation as a function of time. For each scan, the offset $\varphi_{i0}(y)$ could be modified in order to display the signal that would be spatially observed for the corresponding y position. Figure 8 shows the temporal hypertelescope implemented in our laboratory.

Fig 8: General overview of the temporal hypertelescope breadboard.

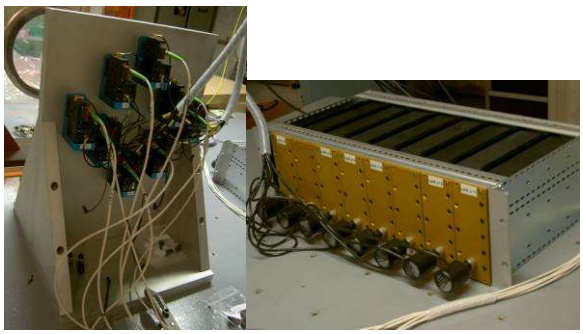

Fig 9: left: telescope array with 8 apertures and the relevant collimating assemblies. right: set of optical fibre modulators and delay lines

In this first demonstration instrument, the target will be 1D in order to simplify the breadboard using single or binary stars as test objects. It consists of a set of monomode fibres fed by DFB lasers and acting as point like sources. The fibres outputs are placed in the focal plane of a collimator. This collimated beam is sampled by a telescope array as shown in the left side of figure 9. Eight small lenses act as telescopes and focus the collected light in the monomode fibre arms. Each fibre arm includes a fibre delay line and an optical fibre modulator able to vary the optical path according to linear variation as function of time with slopes defined in equation (3). This process is achieved using a global driving electronic managed by a Lab View Virtual Instrument.
A 8 to 1 PM coupler allows to recombine the 8 beams. An InGaAs detector provides the final interferometric signal. All over this instrument the birefringence properties are monitored in order to Ensure the polarisation coherence preservation. As long as this preliminary experiment is achieved in a quasi monochromatic configuration, the differential dispersion effects are not significant.
The preliminary results have been obtained on a point-like source in order to characterize the point spread function of the instrument. The servo loop being under design and not available, the results reported in figure 10 have been recorded in an open loop configuration. These experimental results demonstrate the principle of temporal hypertelescopes even if the dynamic of the image remain low due to the instrument instabilities. Using a preliminary apodization of the pupil it as been possible to improve the result by reducing the ripple around the central peak. Side peaks on the edges of figures 10 are related to 1 and -1 interferometric orders. They have been displayed for pedagogic reason. In a real observation, the span of the temporal modulations will be reduced in order to avoid image aliasing.

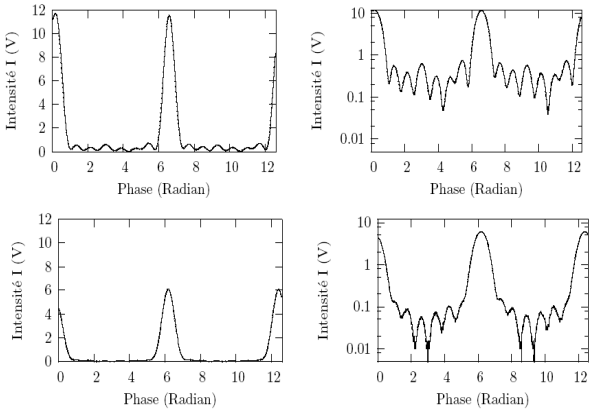

Fig 10 Preliminary results on the temporal hypertelescope PSF. Up: without apodization; down: with a preliminary apodization. Left: linear scale; right log scale.

5 PERSPECTIVES AND CONCLUSIONS

We have proposed a new concept for direct imaging which can overcome the technical difficulties of the classical spatial hypertelescope. A preliminary experiment has been implemented and preliminary encouraging results have been obtained.
Nevertheless, several points should be improved for a full demonstration of the temporal hypertelescope potential.
The first one deals with the stabilization of the instrument. The number of interferometric arms, the redundant or non redundant configuration and the typical $\frac{\lambda}{100} - \frac{\lambda}{1000}$ optical path accuracy makes necessary to propose innovative servo control systems using our background knowledge in this domain. A servo control system based on the simultaneous propagation of a metrology light and the science one could be used. We are also investigating the possibility to process the data thanks to a genetic algorithm. Note that this problem is common with all the phased arrays devoted to high resolution imaging.
The second point to be investigated is related to the optimization of the PSF. In the frame of collaboration with the mathematics department of our institute, we undertake a study on the improvement of the point spread function rejection ratio using mathematical optimization methods. The redundant versus non-redundant input pupil geometry and the pupil apodization process are investigated taking care to find solutions not too much sensitive to the external perturbations.
At last, the present design of our temporal hypertelescope has not been optimized in term of sensitivity. This presentation has been focused on the principle and the related advantages of the temporal modulation and densification using a simple N to 1 combiner for pedagogical reasons. For a future instrument, the N to 1 combiner will not be efficient as long as the N-1 missing outputs lead to a large loss of energy. At the present time, a N to N combiner is under study in our lab. The main goal of this study will be to propose a beam combiner giving rise to a set of outputs with a global preservation of the energy. By this way the temporal hypertelescope will reach the same sensitivity as a spatial one.

Acknowledgment:

This work is supported by the Centre National d'Etude Spatiale (CNES) and Institut des Sciences de l'Univers (INSU/CNRS).

6 REFERENCES

1. A. Labeyrie, A&AS, 118, 517 (1996)
2. F. Vakiliet al, A&A, 421, 147 (2004)
3. W. A. Traub, 1986, Appl. Opt. 25, 528
4. E. Pedretti, et al, A&AS, 147, 285 (2000)
5. S. Gillet et al., A&A, 400, 393 (2003)
6. E. Aristidi et al, SPIE 5491, New Frontiers in Stellar Interferometry, Ed. W.A. Traub, Bellingham, SPIE, 7636 (2004)
7. O. Lardiere et al, MNRAS Vol. 375, Issue 3, pp. 977-988 (2007)
8. R. N. Bracewell, Nature, 274, 780 (1978)
9. Delage et al , Appl. Opt., 39, 6406 (2000)
10. Reynaud et al, Appl. Opt., 31, 19, 3736 (1992)